Powder Technology 246 (2013) 157–168

Contents lists available at SciVerse ScienceDirect

Powder Technology

journal homepage: www.elsevier.com/locate/powtec

Viscoelastic discrete element model of powder sintering

S. Nosewicz [a], J. Rojek [a,*], K. Pietrzak [a,b], M. Chmielewski [b]

[a] Institute of Fundamental Technological Research, Polish Academy of Sciences, Pawińskiego 5B, 02-106 Warsaw, Poland
[b] Institute of Electronic Materials Technology, ul. Wólczyńska 133, 01-919 Warsaw, Poland

ARTICLE INFO

Article history:
Received 29 October 2012
Received in revised form 9 May 2013
Accepted 11 May 2013
Available online 18 May 2013

Keywords:
Powder sintering
Simulation
Discrete element method
Viscoelastic model

ABSTRACT

This paper presents an original viscoelastic model of powder sintering developed within the discrete element framework. The viscous model used by other authors has been enriched by adding a spring connected in series to the viscous rheological element. In this way elastic and viscous effects in the particle interaction during sintering are treated using the Maxwell viscoelasticity. The new numerical model has been verified through simulation of simple problems of free sintering and sintering under pressure. Sintering processes have been treated as isothermic. In order to accelerate the analysis an algorithmic mass scaling has been used allowing to use larger time steps in the explicit time integration scheme. The results obtained using the new model are consistent with the standard viscous model. At the same time, a much better efficiency of the new model in comparison to the standard viscous one has been found because the critical time steps required by the viscoelastic model are much larger than those required by the viscous model. The new model has been applied to the simulation of real process of sintering of NiAl powder. The kinetics of sintering indicated by the evolution of density has been studied. The comparison of numerical and experimental results has shown a good performance of the developed numerical model.

1. Introduction

Sintering is a manufacturing process used for making various parts from metal or ceramic powder mixtures. Sintering consists in consolidation of loose or weakly bonded powders at elevated temperatures, close to the melting temperature with or without additional pressure. Changes of the microstructure during sintering have been shown in Fig. 1. In the initial stage (Fig. 1a) cohesive bonds are formed between particles. When the sintering process is continued, the necks between particles grow due to mass transport (Fig. 1b). Surface and grain boundary diffusion are normally dominant mechanisms of mass transport in a sintering. The main driving force of sintering is reduction of the total surface energy of the system. As a result of the stresses in the neck and the surface tension the particles are attracted to each other, which leads to the shrinkage of the system. The described processes – shrinkage and mass transport – lead to the reduction of material porosity. Sintering is a complex process influenced by many factors including technological ones such as temperature, sintering time, pressure and atmosphere which determine the properties of sintered materials [9,32,65,8].

Modelling can be used to optimize and to understand the sintering process better and improve the quality of sintered components. Modelling of the sintering process is one of the most challenging problems in material modelling. There are different approaches in modelling of sintering processes, ranging from continuum phenomenological models to micromechanical and atomistic ones. Different sintering models have been reviewed in [44,49,16,20]. In the continuum approach, the porous powder under compaction is treated as a continuous medium at the macro-scale. Its deformation behavior is described by constitutive equations based on modified theory of solids. Constitutive equations of continuous media belong to the class of phenomenological models in which model parameters are obtained by fitting experimental data. Well-known phenomenological sintering models are those developed by Abouaf et al. [1], Duva and Crow [13], Cocks [11], Sofronis and McMeeking [58], and Ponte [7]. Phenomenological approaches have been summarized by Olevsky [45], Exner and Kraft [16], Cocks [12] and German [21,23].

Phenomenological theories do not take into consideration the microstructure of the material. Microstructural changes during sintering are taken into account in micromechanical models. A number of micromechanical models of sintering are based on a particle representation of porous powder material undergoing the sintering process. In particle models, the interaction of particles and the local problems of particle necks are considered. Sintering is treated as a collective result of thermally activated adhesion processes which result in the growth of contacts between particles. Sintering models at the particle scale have been used in the classical works on sintering. Frenkel [17] and Kuczynski [37] studied mechanisms of neck growth and shrinkage for the early sintering stages (particle bonding) using a two-sphere model. The two-particle model has been extrapolated for

* Corresponding author.
E-mail addresses: snosew@ippt.gov.pl (S. Nosewicz), jrojek@ippt.gov.pl (J. Rojek), katarzyna.pietrzak@itme.edu.pl (K. Pietrzak), chmielem@poczta.fm (M. Chmielewski).

0032-5910/$ – see front matter © 2013 Elsevier B.V. All rights reserved.
http://dx.doi.org/10.1016/j.powtec.2013.05.020

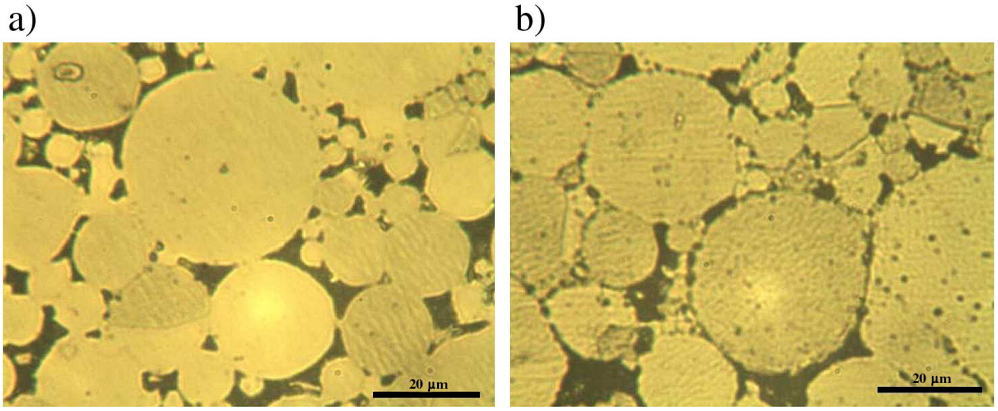

Fig. 1. Microstructure evolution during sintering of NiAl: a) early stage, b) final stage.

the intermediate shrinkage state by Kingery and Berg [35]. Coble [10] developed a cylindrical pore model, a spherical pore model for the late sintering stages was developed by MacKenzie and Shuttleworth [43]. More sophisticated models taking into account the superposition of various sintering mechanisms have been developed by Ashby [4], Arzt [3], and Exner and Arzt [15].

Growing capabilities of computational techniques increased the possibilities to employ particle sintering models. Sintering models have been implemented within the discrete element method which allows us to model interaction of large collections of particles [50,42,41,46,31,25,26,66]. Parhami and McMeeking [50] have implemented the particle sintering model derived by Coble [10] in the quasi-static formulation of the lattice type discrete element method to study free and pressure-assisted sintering. The concepts of Parhami and McMeeking have been incorporated in the dynamic formulation of the discrete element method by Martin et al. [42] and used for investigation of free sintering of metallic powders. A similar model has been applied by Henrich et al. [26] to simulate the free and pressure-assisted solid-state sintering of powders with special attention to the grain rearrangement during sintering. The effect of particle size distributions on sintering has been studied by Wonisch et al. [66]. The two-particle models of sintering implemented within the discrete element method [50,42,66] can represent properly the microstructure of a sintered material at early and intermediate stages of sintering. We can extend its use very carefully to higher densities, but we must remember that for compact solids these models lose their physical background, that is, they no longer represent a microstructure and can be treated as a mere way of discretization [60]. An interesting extension of the particle model for the final stage of sintering has been presented in [31], where the transformation of the particle model to a polyhedral one at a certain level of the process was proposed.

The macroscopic behavior of sintered materials is a result of a complex combination of elastic, viscous, plastic and thermal deformation depending on the processes occurring at the microscopic and atomistic levels [67,6]. Different deformation mechanisms dominate at different stages of a powder metallurgy process [2]. Although deformation during sintering itself is governed mainly by the viscosity, the material does maintain certain elasticity [39,38]. Phenomenological sintering models generally incorporate mechanisms of thermal and elastic deformation along with the viscous creep flow [19,67,30,34] although there is little knowledge of elastic properties during sintering. Experimental data on elastic properties at high temperatures in most cases do not cover the temperature ranges of sintering [40]. Due to insufficient data, elastic deformation in sintering models in most cases has been simply approximated in constitutive models of sintering [22,23]. Accounting for elastic effects may be important for a proper evaluation of stresses and reversible strains during sintering [34]. Experimental measurements such as those presented in [39,38] show important changes in the value of the Young's modulus during sintering and allow us to hope that future experimental investigation will enable a better understanding of elastic effects during sintering.

In the discrete element models of powder metallurgy process cited above, cf. [50,26,66,46], the sintering stage has been modelled assuming the viscous flow and neglecting elastic behavior. This paper presents a consistent viscoelastic model of particle interaction which allows us to keep elastic and viscous components of deformation. Accounting for elastic effects may influence the distribution of forces in the heterogeneous particulate material and have some importance to the evaluation of stresses during sintering and subsequent cooling.

The new sintering model has been implemented in the authors' own discrete element code [53,56,48,55,54]. The numerical model is verified by simple tests of two particle sintering as well as by more realistic tests of sintering of a cylindrical specimen composed of several hundred particles. The performance of the new viscoelastic model has been compared with that of the standard viscous model. While general agreement in the results has been observed, it has been found that the new model offers a much better numerical efficiency since it enables the use of a much larger time step in an explicit time integration of equations of motion. This is an important advantage of the newly developed model.

2. Numerical model of sintering

Numerical model of sintering is developed within the framework of the discrete element method which assumes that a particulate material can be represented as a collection of spherical particles interacting with one another. Following Martin et al. [42] the rotational motion of the particles and tangential interaction has been neglected in the present formulation. This should be favorable for particle rearrangements. Nevertheless, further development of the model should include tangential forces as well as the moment interaction between particles.

2.1. Discrete element formulation

The translational motion of rigid particles is described by means of the Newton's equations of rigid body dynamics. For the i-th element we have

$$m_i \mathbf{u}_i = \mathbf{F}_i, \tag{1}$$

where $\mathbf{u}_i$ is the element centroid displacement in a fixed (inertial) coordinate frame, $\mathbf{m}_i$ — element (particle) mass, and $\mathbf{F}_i$ — the resultant force being the sum of all the forces applied to the i-th element due

to the external load, $\mathbf{F}_i^{\text{ext}}$, and contact interactions with neighboring spheres and boundary surfaces $\mathbf{F}_{ij}^{\text{cont}}$

$$\mathbf{F}_i = \mathbf{F}_i^{\text{ext}} + \sum_{j=1}^{n_i^c} \mathbf{F}_{ij}^{\text{cont}}, \tag{2}$$

where n_i^c is the number of elements being in contact with the i-th discrete element. Contact forces $\mathbf{F}_{ij}^{\text{cont}}$ are obtained using a constitutive model formulated for the interaction of two particles. Below, we present interaction models for powder compaction and sintering. In further considerations, in order to simplify the notation the indices i and ij are omitted.

2.2. Contact interaction model for powder compaction

Powder compaction prior to sintering is modelled using the cohesionless contact model whose rheological scheme is shown in Fig. 2. The contact interaction is represented by the Kelvin–Voigt element consisting of a spring and a dashpot connected in parallel. The contact force F^{cont} is a sum of the elastic force in the spring F^{e} and the viscous component F^{d}

$$F^{\text{cont}} = F^{\text{e}} + F^{\text{d}}. \tag{3}$$

The elastic part of the contact force F^{e} can be evaluated assuming a linear force–displacement relationship

$$F^{\text{e}} = k u_{\text{rn}}, \tag{4}$$

where k is the contact stiffness and u_{m} is the penetration of the particles. No cohesion, and thus no tensile contact forces are allowed, i.e. $F^{\text{e}} \le 0$.

The viscous component is assumed to be a linear function of the normal relative velocity v_{rn}

$$F^{\text{d}} = c v_{\text{rn}}. \tag{5}$$

The value of the viscosity coefficient c can be taken as a fraction ξ of the critical damping C_{cr} for the considered system

$$c = \xi C_{\text{cr}}. \tag{6}$$

The critical damping for the system of two rigid bodies with the masses of m_i and m_j, connected with a spring with the stiffness k can be calculated as, cf. [61]:

$$C_{\text{cr}} = 2\sqrt{\frac{m_i m_j k}{m_i + m_j}}. \tag{7}$$

2.3. Viscous model of sintering

The model of particle interaction during free sintering must take into account adhesion between grains of a sintered material. The model adopted for free sintering is based on the classical models developed at particle level [10,27,28] and used in previous implementations in the discrete element method, cf. [50,42,46]. The particle interaction force, F, during sintering is given by the equation derived considering mass transport and stresses at the grain boundary between two sintered particles, cf. [28,50,42]:

$$F = \frac{\pi a^4}{8 D_b} v_{\text{rn}} + \pi \gamma_S \left[4r\left(1 - cos\frac{\Psi}{2}\right) + asin\frac{\Psi}{2} \right] \tag{8}$$

where v_{rn} — the normal relative velocity, r — the particle radius, a — the radius of the interparticle grain boundary, Ψ — the dihedral angle, γ_s — the surface energy and D_b — the effective grain boundary diffusion coefficient. The geometrical parameters of the model are defined in Fig. 3. The dihedral angle Ψ can be determined from the balance of surface tensions at the grain boundary tri-junction at the phase equilibrium [64]. The effective diffusion coefficient is given by the following equation, cf. [50]:

$$D_b = \frac{D_g \delta_g \Omega}{kT} \tag{9}$$

where Dg — diffusion coefficient, δ_g — thickness of the grain boundary, Ω — atomic volume, k — Boltzmann constant, T — sintering temperature.

The initial neck radius a_0 depends on the initial penetration u_{rn}^0 induced by the compaction. From simple geometrical considerations we have

$$a_0 = \sqrt{\frac{r u_{\text{rn}}}{2}}. \tag{10}$$

The growth of the radius of the interparticle grain boundary is governed by the following evolution law:

$$\dot{a} = -\frac{r v_{\text{rn}}}{a}. \tag{11}$$

The grain boundary radius a grows until the sintering process is stopped. Its maximum at the equilibrium state is given by the following geometric relationship:

$$a_{\max} = rsin\frac{\Psi}{2}. \tag{12}$$

The model described by Eq. (8) has been derived for identical particles. Following [42] it can be generalized to the sintering of different size particles by replacing the radius r in Eqs. (8)–(12) with the equivalent particle radius $\bar{r}$ given by the following formula:

$$\bar{r} = \frac{2 r_i r_j}{r_i + r_j}. \tag{13}$$

On the right-hand side of Eq. (8) we have two terms, the first one has a character of viscous resistance to the particle approaching

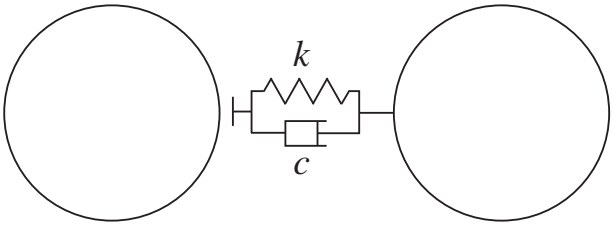

Fig. 2. Rheological scheme of the contact interaction for powder compaction.

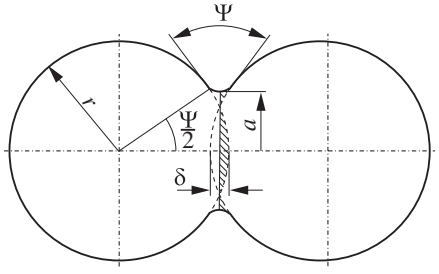

Fig. 3. Two-particle model of sintering.

caused by the sintering attracting force represented by the second term. These force components denoted as, F^{v} and F^{sint}, respectively, can be expressed, accordingly, as:

$$F^{v} = \eta v_{rn} \tag{14}$$

where the viscosity η is given by

$$\eta = \frac{\pi a^4}{8 D_b} \tag{15}$$

and

$$F^{sint} = \pi \gamma_S \left[4r\left(1 - cos\frac{\Psi}{2}\right) + asin\frac{\Psi}{2} \right]. \tag{16}$$

The decomposition of the interaction force in the sintering model can be represented by the rheological scheme shown in Fig. 4.

2.4. Viscoelastic model of sintering

The rheological model of sintering presented above can be enriched by adding an elastic component. This allows us to account better for material properties which are characterized by a certain elasticity during sintering, as well. The elastic component allows us to consider more accurate redistribution of the forces in the particle assembly with large changes of configuration during sintering. Seeing an analogy of a sintered material with a fluid, whose viscoelastic properties are commonly modelled with the viscoelastic Maxwell model, we introduce the elastic component in series with the viscous element. In this way, the rheological scheme presented in Fig. 5 is obtained.

For the Maxwell element we have the following relationships for forces and velocities:

$$F^{v} = F^{e} \tag{17}$$

$$v_{rn} = v^{v}_{rn} + v^{e}_{rn}. \tag{18}$$

Equation (17) means that the forces transferred through the spring and viscous component, F^{e} and F^{v}, respectively, are equal. Equation (18) expresses the additive decomposition of the relative normal velocity between particles v_{rn} into the elastic and viscous parts, v^{e}_{rn} and v^{v}_{rn}, respectively. Expressing the viscous and elastic forces analogously to Eqs. (14) and (4), and substituting these relationships into (18), we obtain the evolution equation for the force in the Maxwell branch

$$v_{rn} = \frac{\dot{F}^{e}}{k} + \frac{F^{v}}{\eta}. \tag{19}$$

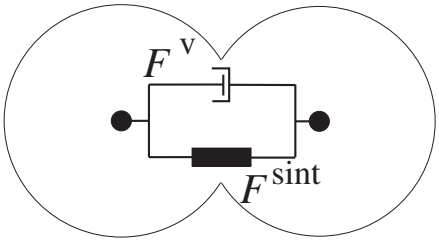

Fig. 4. Rheological scheme of the viscous model of free sintering.

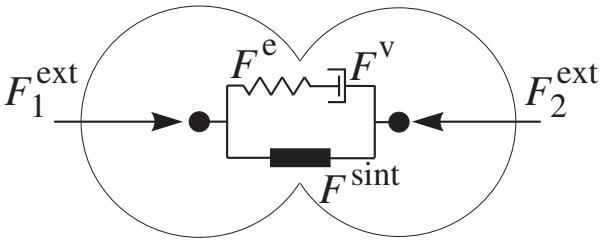

Fig. 5. Rheological scheme of the viscoelastic model of sintering under pressure.

2.5. Transition between Kelvin–Voigt and Maxwell models

In the process in question, we deal with different material behavior, changing in time. During powder compaction the material has a solid-like behavior while during sintering it attains fluid-like behavior. A certain analogy to this change of properties can be seen in solid–liquid transitions occurring during melting [33] or in polymers undergoing the glass transition [52,36,18].

According to the main characteristics of the material different viscoelastic models have been adopted here for the two types of material behavior of powder material during the manufacturing process involving pressing and sintering. The powder material during pressing is modelled with the Kelvin–Voigt element (Section 2), which is better suited to describe the nature of a solid material. The irreversible flow during sintering is represented better using the model with the nonlinear Maxwell element presented in Section 4.

Transition from the solid-like to fluid-like behavior and simultaneous change of the model type are associated with a sharp change of viscoelastic properties. In order to smoothen the transition we introduce a gradual smooth change of parameters at a certain time interval $(t_0, t_0 + t_{rel})$, where t_0 is the time when sintering is initiated. At this interval the viscosity coefficient η in the Maxwell element changes according to the following function:

$$\eta = \eta_{\infty}(1 - \varepsilon) + \varepsilon \eta_{teor} \tag{20}$$

where η_{∞} is the viscosity coefficient in the Maxwell element before sintering, η_{teor} is the theoretical viscosity calculated according to the formula (15), and $\varepsilon \in < 0,1 >$ is a coefficient ensuring gradual change of η from η_{∞} at $t = t_0$ to η_{teor} at $t = t_0 + t_{rel}$. The smooth transition is obtained by the following definition of ε:

$$\varepsilon = \frac{1 - cos\alpha}{2}, \quad \text{where} \quad \alpha = \frac{t - t_0}{t_{rel}}\pi, \quad t \in < t_0, t_0 + t_{rel} > . \tag{21}$$

If we assume that the Maxwell element is used before sintering when we deal with an elastic material, its viscosity coefficient would have a very high value. In our model we prescribe this value arbitrarily taking a certain value based on numerical tests.

In order to avoid step-type loading the sintering force is also scaled with a smoothly increasing function from 0 to 1 at the time interval $< t_0, t_0 + t_{rel} >$:

$$F^{sint} = \varepsilon F^{sint}_{teor} \tag{22}$$

where ε is defined by Eq. (21) and F^{sint}_{teor} is evaluated according to Eq. (16).

If simulation of the process is continued after the condition of equilibrium given by Eq. (12) is achieved, we have also a sharp change of properties. We keep using the Maxwell model, but we change properties setting a higher value of the viscosity parameter η and set to zero the sintering force F^{sint}. In order to smoothen the changes of the model parameters, we use a similar scaling of the

viscosity coefficient and the sintering force at a certain time interval after the end of sintering:

$$\eta = \varepsilon'\eta_\infty + \left(1-\varepsilon'\right)\eta_{\text{teor}} \tag{23}$$

$$F^{\text{sint}} = \left(1-\varepsilon'\right)F^{\text{sint}}_{\text{teor}} \tag{24}$$

with

$$\varepsilon' = \frac{1-cos\alpha'}{2}, \quad \text{where} \quad \alpha' = \frac{t-t_{\text{end}}}{t_{\text{rel}}}\pi, \quad t\in<t_{\text{end}}, t_{\text{end}}+t_{\text{rel}}> \tag{25}$$

and t_{end} is the time when the condition of equilibrium given by Eq. (12) is achieved.

2.6. Time integration scheme

The Eqs. of motion (1) are integrated in time using an explicit central difference type algorithm, the so-called leap-frog method:

$$\mathbf{u}_i^n = \frac{\mathbf{F}_i^n}{m_i}, \tag{26}$$

$$\mathbf{u}_i^{n+1/2} = \mathbf{u}_i^{n-1/2} + \mathbf{u}_i^n \Delta t, \tag{27}$$

$$\mathbf{u}_i^{n+1} = \mathbf{u}_i^n + \mathbf{u}_i^{n+1/2}\Delta t, \tag{28}$$

where accelerations, $\mathbf{u}_i^n$, and positions, $\mathbf{u}_i^n$ and $\mathbf{u}_i^{n+1}$, are defined at time instants t^n and t^{n+1} ($t^{n+1} = t^n + \triangle t$), while velocities $\mathbf{u}_i^{n-1/2}$ and $\mathbf{u}_i^{n+1/2}$ are shifted by a half-step.

Eqs. (26)–(28) give a new configuration at time instant t^{n+1}. In order to pass to the next step, forces at this configuration must be evaluated. First step in the calculation of force interactions in sintering for both presented models is updating the radius of the interparticle grain boundary according to the evolution law given by Eq. (11). We take Eq. (11) at the midpoint at time instant $t^{n+1/2}$

$$\dot{a}^{n+1/2} = -\frac{rv_{\text{rn}}^{n+1/2}}{a^{n+1/2}} \tag{29}$$

in which we employ the following central difference schemes:

$$\dot{a}^{n+1/2} = \frac{a^{n+1}-a^n}{\Delta t} \tag{30}$$

$$a^{n+1/2} = \frac{a^{n+1}+a^n}{2}. \tag{31}$$

The new radius a_{n+1} can be solved in terms of known parameters as:

$$a^{n+1} = \sqrt{(a^n)^2 - 2rv_{\text{rn}}^{n+1/2}\Delta t}. \tag{32}$$

In the convention adopted, the relative velocity in a sintering process is negative when the two particles are getting closer, so the second term under square root in Eq. (32) is positive.

Substituting the new radius a^{n+1} into Eq. (16) we evaluate the sintering driving force $(F^{\text{sint}})^{n+1}$ at time instant t_{n+1} for both the viscous and viscoelastic model.

The viscous part of the interaction force in the viscous model is computed taking Eq. (14) at time instant $t^{n+1/2}$

$$\left(F^{\text{v}}\right)^{n+1/2} = \eta^{n+1/2}v_{\text{rn}}^{n+1/2}. \tag{33}$$

Using the midpoint rule

$$\left(F^{\text{v}}\right)^{n+1/2} = \frac{\left(F^{\text{v}}\right)^{n+1}+\left(F^{\text{v}}\right)^n}{2} \tag{34}$$

we obtain the expression for the viscous resistance at time instance t_{n+1}

$$\left(F^{\text{v}}\right)^{n+1} = 2\eta^{n+1/2}v_{\text{rn}}^{n+1/2} - \left(F^{\text{v}}\right)^n. \tag{35}$$

For the viscoelastic sintering model we take Eq. (19) at the time instant $t^{n+1/2}$:

$$v_{\text{rn}}^{n+1/2} = \frac{\left(\dot{F}^{\text{e}}\right)^{n+1/2}}{k} + \frac{\left(F^{\text{v}}\right)^{n+1/2}}{\eta^{n+1/2}}. \tag{36}$$

Accounting for the equality (17) and substituting the following finite difference expressions:

$$\left(\dot{F}^{\text{e}}\right)^{n+1/2} = \frac{\left(\dot{F}^{\text{e}}\right)^{n+1}-\left(\dot{F}^{\text{e}}\right)^n}{\Delta t} = \frac{\Delta F^{\text{e}}}{\Delta t} \tag{37}$$

$$\left(F^{\text{e}}\right)^{n+1/2} = \left(F^{\text{e}}\right)^n + \frac{\Delta F^{\text{e}}}{2} \tag{38}$$

into Eq. (36) we obtain the expression for the new value of the force in the Maxwell element

$$\left(F^{\text{e}}\right)^{n+1} = \frac{v_{\text{rn}}^{n+1/2}\Delta t + \left(F^{\text{e}}\right)^n\left(\frac{1}{k}-\frac{\Delta t}{2\eta^{n+1/2}}\right)}{\frac{1}{k}+\frac{\Delta t}{2\eta^{n+1/2}}}. \tag{39}$$

The integration scheme given by Eq. (39) corresponds to the trapezoidal or two-stage Lobatto IIIA method of integration [59]. Other possible integration methods of the viscoelastic Maxwell model can be found in [59].

2.7. Numerical stability and mass scaling

Explicit time integration scheme given by Eqs. (26)–(28) is characterized by a high efficiency of the solution at each time step. The equations are decoupled and there is no need to solve a system of algebraic equations or perform iterations. The known drawback of the explicit time integration scheme is its conditional numerical stability which imposes the limitation on the time step $\triangle t$, i.e.

$$\Delta t \leq \Delta t_{\text{cr}} \tag{40}$$

where $\triangle t_{\text{cr}}$ is the critical time step. For a system of two masses m connected by a spring with the stiffness k the critical time step is given by:

$$\Delta t_{\text{cr}} = \frac{2}{\omega} \tag{41}$$

where

$$\omega = \sqrt{\frac{2k}{m}} \tag{42}$$

is the angular eigenfrequency of the considered system.

The critical time for the system of two masses m connected by a Kelvin element (a spring k in parallel with a damper c) corresponding to two particles during compaction is given by

$$\Delta t_{\text{cr}} = \frac{2}{\omega}\left(\sqrt{1+\xi^2}-\xi\right) \tag{43}$$

where ξ is the damping ratio introduced in Eq. (6).

Table 1
Material data for copper sintering (T = 1300 K) according to [50].

Material constant	Parameter value
Diffusion coefficient, $D_g\delta_g$	$3.832 \cdot 10^{-29}$ m^3/s
Atomic volume, Ω	$1.18 \cdot 10^{-29}$ m^3
Surface energy γ_s	1.72 J/m^2
Dihedral angle Ψ	146°

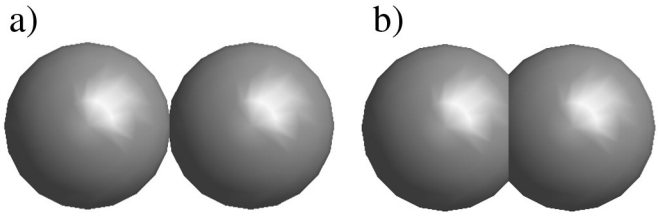

Fig. 6. Simulation of sintering of two particles: a) initial configuration, b) end of sintering.

The critical time step for the system of two masses m connected with a damper with the viscosity η is determined from the following formula:

$$\Delta t_{cr} = \frac{2m}{\eta}. \tag{44}$$

The stability of discrete systems with Maxwell elements has been studied in [24]. The critical step for the system of two masses m connected by a Maxwell element consisting of a spring with the stiffness k and a damper with the viscosity η can be evaluated in a simple way, cf. [51], as the minimum

$$\Delta t_{cr} = \min\{\tau_\omega, \tau_{Mr}\} \tag{45}$$

of the critical time step τ_ω resulting from undamped vibrations with the angular frequency ω determined from Eq. (42)

$$\tau_\omega = \frac{2}{\omega} \tag{46}$$

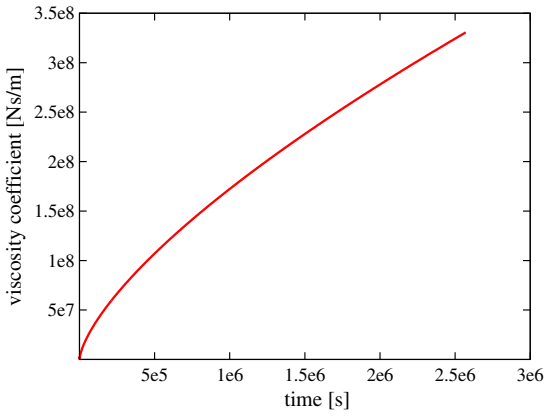

Fig. 8. Evolution of the viscosity coefficient at free sintering of two grains of Cu.

and the Maxwell relaxation time τ_{Mr} defined as:

$$\tau_{Mr} = \frac{\eta}{k}. \tag{47}$$

Evaluation of the critical time step for a multi-body discrete system requires the consideration of the whole set of differential equations. This is not efficient for large models of discrete elements, therefore simpler methods to calculate the stability limit are necessary [47]. In practice, the critical time step in discrete element models is taken as the minimum of the values obtained for all the connections considered separately and multiplied by a certain safety factor β

$$\Delta t \le \beta \Delta t_{cr} \tag{48}$$

where $0 < \beta < 1$. The value of β has been studied by different authors. A good review can be found in [47], where the value close to 0.17 is recommended for 3D simulation and 0.3 — for a 2D case.

The values of critical time steps are usually relatively small, so simulation with an explicit time integration usually requires the use of large number time steps. Therefore, this approach is most suitable for transient and high speed problems. Simulation of longer and low speed processes could be too expensive. A possible way around consists in artificial density or mass scaling in order to increase the critical time step

$$m' = \alpha_m m \tag{49}$$

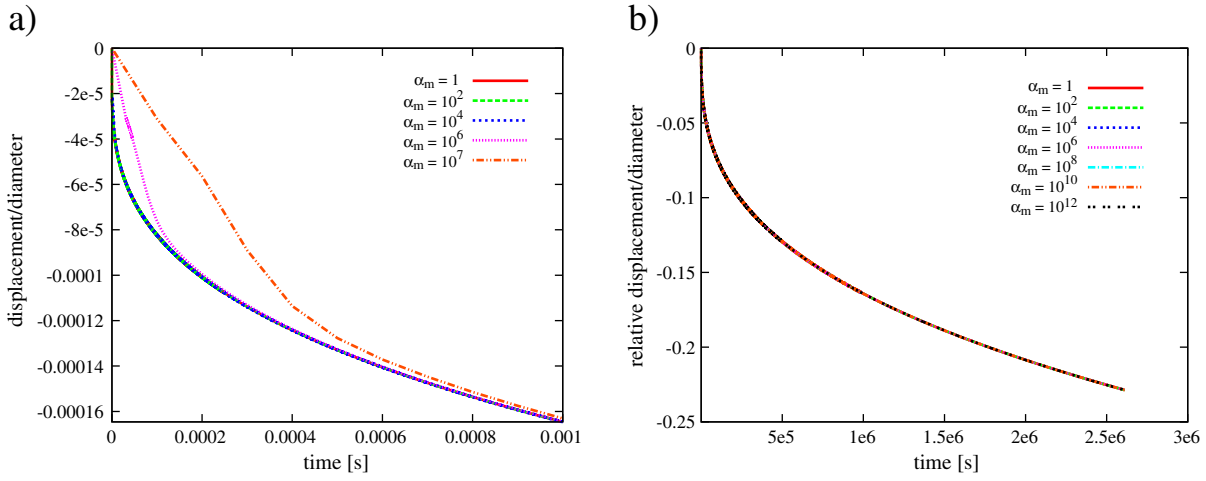

Fig. 7. Simulation of sintering of two particles using the viscous model. Evolution of displacement and effect of mass scaling: a) initial period of the process, b) the whole process.

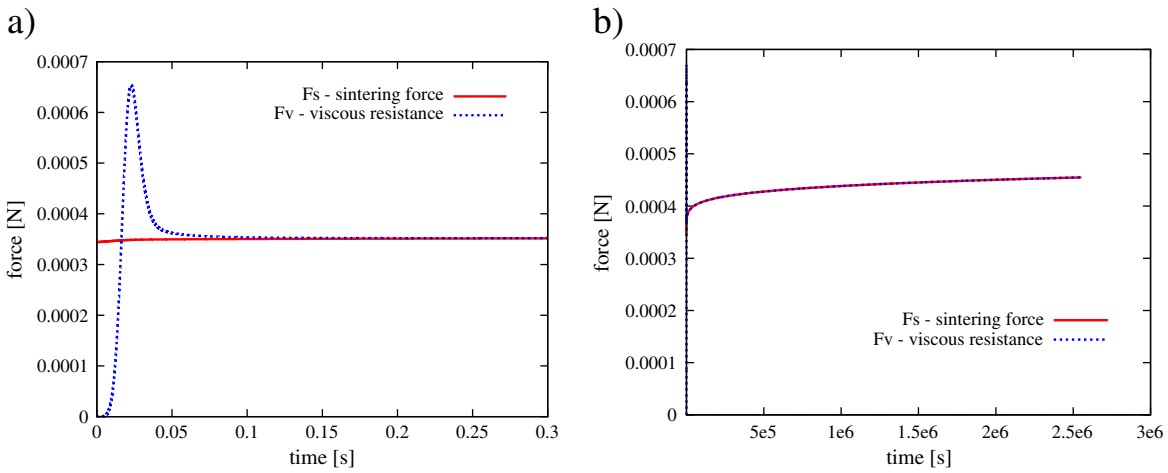

Fig. 9. Evolution of sintering force and viscous resistance at free sintering of two grains of Cu (mass scaling factor 10^{14}): a) initial period of the process, b) the whole process.

where m is the real mass, α_m is the mass scaling factor and m' is the scaled mass. This method is widely used in explicit finite element simulations [29] as well as in the discrete element analyses [62,63].

In general, scaling of equations describing different physical phenomena is performed in such a way that the similarity between the original and scaled models defined by certain dimensionless numbers is satisfied [5]. Employing the notions from fluid dynamics, we can notice that the mass scaling performed according to Eq. (49) with other quantities unchanged does not ensure the dynamic similarity governed by the ratio of the inertial to viscous forces. However, it is assumed that inertial effects (inertial terms in equations of motion) in the considered problem are so small that even a large upscaling of mass and the resulting increase of the inertial terms will not significantly affect the solution. The value of the scaling factor depends on the problem. It is indicated in [63] that mass can be scaled by factors greater than 10^{10} in quasi-static DEM simulations.

Sintering processes are very slow and time steps allowed in explicit simulation are very short because of small particle inertia [26]. Sintering can be analyzed efficiently only employing a scaling procedure in the discrete element model. It has been shown in [26] that the particle inertia in a DEM sintering model can be scaled by several orders of magnitude without affecting particle positions. The DEM solution with mass scaling has been verified there by comparison with the solution obtained assuming the zero inertial terms in the governing equations. Similarly, in this work, mass scaling is used. The effect of scaling and correctness of the solution is verified through comparing the solutions with different mass scaling. The convergence of the scaled solution to the solution with real parameters proves that scaling is acceptable.

3. Numerical examples

3.1. Simulation of free sintering

Free sintering of two copper particles of 22.5 μm at temperature 1300 K has been simulated using the model parameters given in Table 1 taken from [50]. Both viscous and viscoelastic models have been used. Fig. 6 shows the particles before and after sintering. The purpose of this numerical test is to: (i) verify the performance of the model for an elementary system, (ii) check mass scaling, (iii) compare results obtained using the viscous and viscoelastic models, (iv) compare the efficiency of the viscous and viscoelastic model, and (v) calculate corresponding relative density evolution of a regular particle assembly and compare it with experimental results from [14].

3.1.1. Simulation of free sintering by means of the viscous model

Figs. 7–9 show the results obtained using the viscous model. Fig. 7 presents the displacement normalized with respect to the particle diameter plotted as functions of time for different mass scaling factors. Except for a very short initial period (Fig. 7a), displacements for different mass scaling practically coincide during most of the sintering period (Fig. 7b). The displacements at the initial stage are small and not significant when compared to the total displacements during sintering. This proves that mass scaling factors employed in the analysis are acceptable.

Fig. 8 presents the evolution of the viscosity coefficient η calculated according to Eq. (15). It can be seen that the value of η is growing due to the growth of the neck which has an adverse effect on the critical time step length evaluated according to Eq. (44). The growth of η

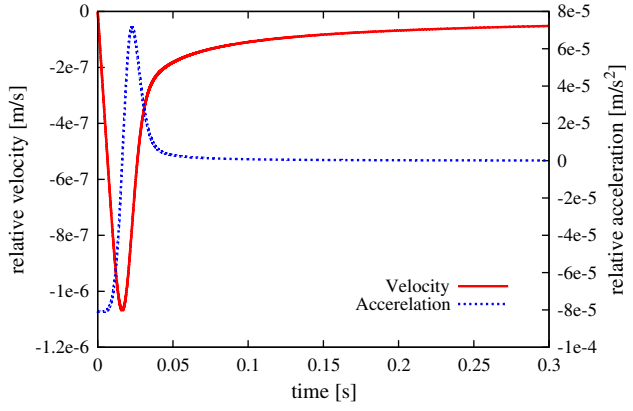

Fig. 10. Evolution of velocity and acceleration at the initial stage of free sintering of two grains of Cu (mass scale factor 10^{14}).

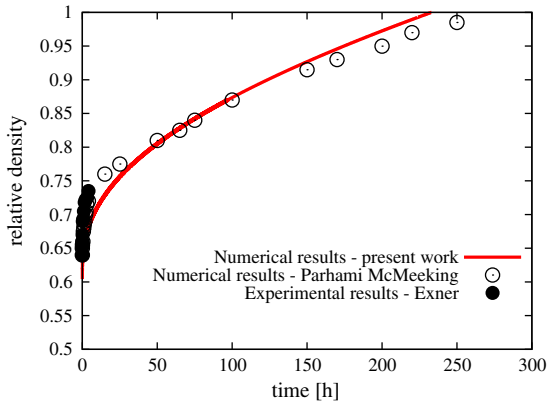

Fig. 11. Evolution of relative density — comparison with numerical results from [50] and experimental ones from [14].

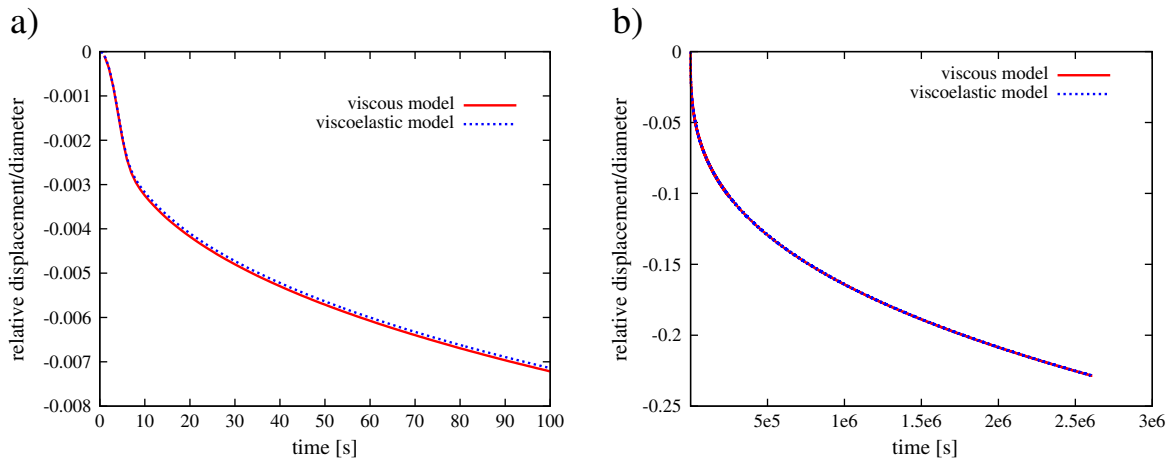

Fig. 12. Evolution of relative displacement at free sintering of two grains of Cu (mass scale factor 10^{14}) — comparison of the viscous and viscoelastic model: a) initial period of the process, b) the whole process.

results in a larger viscous resistance. The viscous resistance and sintering forces are plotted as functions of time in Fig. 9a and b for the initial stage of sintering and for the whole sintering process, respectively. It can be observed that initially the sintering force has a higher value, and this explains a fast increase of the absolute value of relative velocity at this time which is shown in Fig. 10. The viscous resistance is growing due to the increase of the velocity and viscosity. When the viscous resistance becomes higher than the sintering driving force, the velocity starts to decrease. A decreasing velocity in turn causes a decrease in the viscous resistance. Finally, the two forces get very close. Due to a very small difference between these forces the resultant force is very small, which explains a slow rate of changes occurring during sintering.

The relative displacement plotted in Fig. 7a and b is identical with the linear strain

$$e = \frac{\Delta L}{L_0} \tag{50}$$

where L_0 is the initial length of a body subjected to deformation. Let us consider a regular body centered cubic (BCC) packing of identical spheres. The average density $\overline{\rho}_0$ of the BCC packing is $\pi\sqrt{3}/8 \approx 0.68$ [57]. If such an assembly undergoes sintering considered above, we have an isotropic deformation characterized with the strain e in any direction. The corresponding volumetric strain can be calculated as:

$$e_v = \frac{\Delta V}{V_0} = \frac{L_0^3(1+e)^3 - L_0^3}{L_0^3} = (1+e)^3 - 1. \tag{51}$$

The relative density during sintering $\overline{\rho}$ can be easily calculated as:

$$\overline{\rho} = \overline{\rho}_0 \frac{1}{(1+e)^3}. \tag{52}$$

Using the formula (52) we can determine the evolution of the relative density during isotropic sintering characterized with linear strain (shrinkage) plotted in Fig. 7a. The result is presented in Fig. 11 in comparison with the simulation results from [50] and experimental data from [14]. It can be seen that in a simple way we have obtained the evolution of the relative density which is in quite a good agreement with the reference results.

3.2. Simulation of free sintering by means of the viscoelastic model

The problem of sintering of two copper particles previously defined has also been analyzed using the viscoelastic model. The set of material data given in Table 1 has been completed with the spring

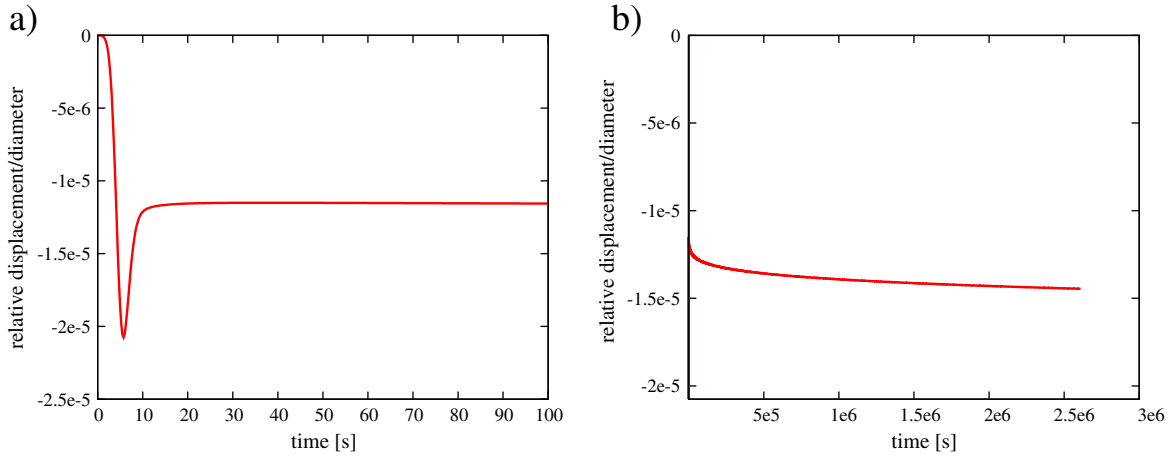

Fig. 13. Evolution of relative elastic displacement at free sintering of two grains of Cu (mass scale factor 10^{14}): a) initial period of the process, b) the whole process.

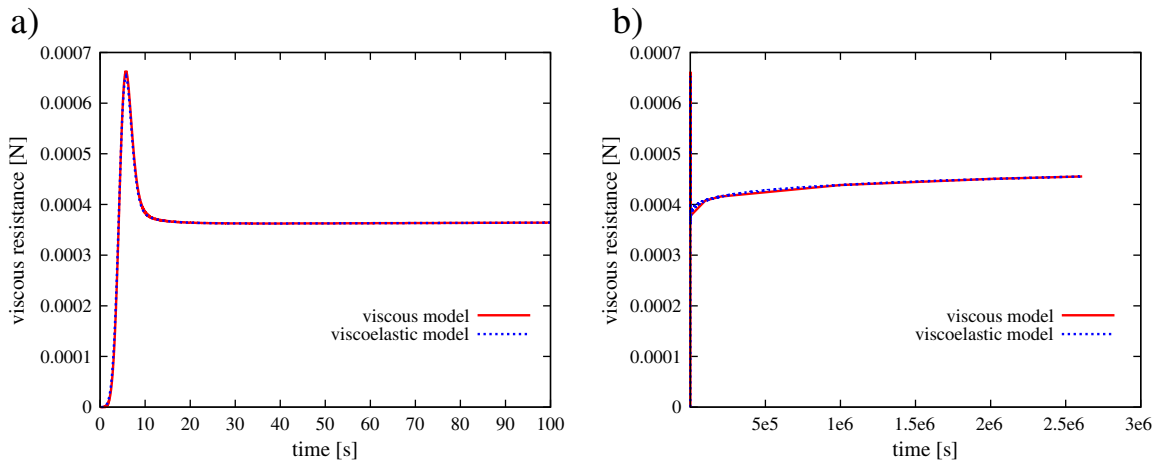

Fig. 14. Evolution of the viscous resistance at free sintering of two grains of Cu (mass scale factor 10^{14}): a) initial period of the process, b) the whole process.

stiffness $k = 7.10^5$ N/m. Taking a cylindrical bar of length and diameter both equal $2r$ as an equivalent element to the considered two-particle system, we can determine the Young's modulus E corresponding to the stiffness k

$$E = \frac{2kr}{\pi r^2} = \frac{2k}{\pi r} = \frac{2 \cdot 7 \cdot 10^5}{\pi \cdot 22.5 \cdot 10^{-6}}\,\text{Pa} \approx 2 \cdot 10^{10}\,\text{Pa}$$

which is a reasonable value for copper at elevated temperature [40].

Fig. 12 shows displacement curves as functions of time obtained using the viscous and viscoelastic models for the same mass scaling. It can be seen that the curves from both models practically coincide. It is understandable because the elastic part of displacements is very small (Fig. 13) while the viscous part in the viscoelastic model should be similar to the displacements in the viscous model. The coincidence of the curves in Fig. 12a and b confirms the correctness of the implementation of the viscoelastic model. The correctness is also verified by the agreement of the curves in Fig. 14a and b representing viscous resistance obtained using both models.

A large difference between the two models can be seen when the computational efficiency is considered. Simulation using the viscoelastic model requires much less time than the one performed by means of the viscous model. The time integration of the viscoelastic model allows the use of much larger time steps, which is illustrated in Fig. 15 showing the evolution of critical time steps in both models for mass scaling factors 10^{14} and 10^{16}. The process is characterized with variable viscosity, therefore the critical time step varies during the simulation. The critical time step for the viscous model estimated according to Eq. (44) is compared with time step limitations for the viscoelastic models used in the formula (45). It can be observed that the time integration of the viscous model allows larger time steps at the very beginning, but the critical time step decreases rapidly due to the increase of viscosity, cf. Fig. 8. The time integration of the viscoelastic model requires smaller time steps in the initial stage when the time step is limited by the relaxation time of the Maxwell element calculated according to Eq. (47). With the growing relaxation time the critical time step increases until the relaxation time becomes larger than the limitation imposed by undamped vibrations. From this moment the critical time step is controlled by Eq. (42) and it is constant until the end of sintering. The interval when the critical time step in the viscoelastic model is restricted by the relaxation time is short in comparison with the rest of the process time. Therefore the efficiency of the process depends primarily on the value obtained from Eq. (42). As it can be observed this value is larger than the critical time step for the viscous model. This guarantees much better efficiency of the viscoelastic model in comparison with the viscous one. Analysis data for two values of mass scaling factor are summarized in Tables 2 and 3. In both cases the number of time steps required for the viscous model and resulting computation times are much larger than respective values for the viscoelastic model. Computation effort at a

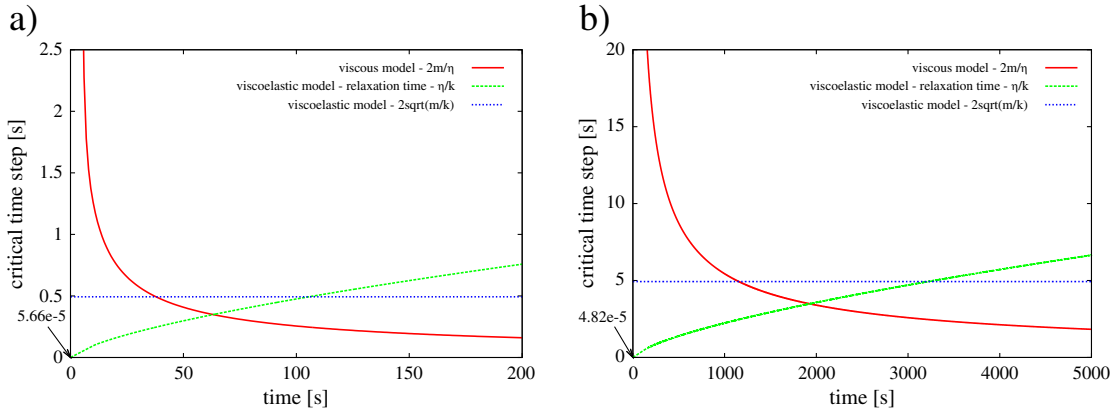

Fig. 15. Comparison of critical time steps for the viscous and viscoelastic models at the initial stage of free sintering of two grains of Cu: a) mass scale factor 10^{14}, b) mass scale factor 10^{16}.

Table 2
Summary of the analysis data for the mass scaling factor 10^{16}.

Model	Sintering time [s]	Number of time steps	Time step 1length [s]	CPU [s]	CPU/step [s]
Viscous	$2.61 \cdot 10^{6}$	$2.61 \cdot 10^{8}$	$10^{-1} \div 10^{-2}$	17	$6.5 \cdot 10^{-8}$
Viscoelastic	$2.61 \cdot 10^{6}$	$9.73 \cdot 10^{5}$	$4.10^{-5} \div 4$	0.12	$1.2 \cdot 10^{-7}$

Table 3
Summary of the analysis data for the mass scaling factor 10^{14}.

Model	Sintering time [s]	Number of time steps	Time step length [s]	CPU [s]	CPU/step [s]
Viscous	$2.61 \cdot 10^{6}$	$2.61 \cdot 10^{10}$	$10^{-3} \div 10^{-4}$	1355	$5.2 \cdot 10^{-8}$
Viscoelastic	$2.61 \cdot 10^{6}$	$6.63 \cdot 10^{6}$	$10^{-5} \div 0.4$	0.9	$1.3 \cdot 10^{-7}$

Fig. 16. Sintered NiAl specimens.

single step for the viscous model is two times smaller than for the viscoelastic model but this does not compensate a much higher number of time steps. This demonstrates clearly the advantage offered by the newly developed viscoelastic model.

3.3. Validation of the model of sintering under pressure

The viscous and viscoelastic models of sintering have been validated using the results of laboratory tests of sintering of NiAl powder.

Table 4
Material data for NiAl sintering ($T = 1573$ K).

Material constant	Parameter value
Diffusion coefficient, $D_g\delta_g$	$2.013 \cdot 10^{-9}$ m^3/s
Atomic volume, Ω	$1.21 \cdot 10^{-29}$ m^3
Surface energy, γ_s	1.58 J/m^2
Dihedral angle, Ψ	150°
Density, ρ	5910 kg/m^3

Sintering has been performed at the temperature 1300 °C (1573 K) under the pressure of 5 and 30 MPa. The sintered specimens are shown in Fig. 16. The process was interrupted at different time instants to perform microscopic observations (Fig. 1) and to measure bulk density. The density evolution, strictly related to sintering kinetics, has been used in the validation of the developed numerical models of sintering.

Maintaining the original grain size (mean radius 11.98 μm), a cylindrical container of diameter 200 μm has been filled with 650 particles (Fig. 17a). It has been assumed that such a reduced geometric model represents correctly sintering process in a real specimen with the diameter of 120 mm. This assumption is justified provided the parameters characterizing sintering are uniformly distributed in a real specimen volume.

The particles in equilibrium under gravity (Fig. 17a) have been subjected to a linearly rising compressive pressure of the rigid punch until the final load has been achieved (Fig. 17b). Then sintering process has been activated and further reduction of the specimen height has been obtained (Fig. 17c).

The problem has been analyzed using the viscous and viscoelastic models. The model has been calibrated for the pressure of 5 MPa and then applied to the simulation of sintering under the pressure of 30 MPa. The model parameters are given in Table 4. In the calibration procedure, the effective diffusion coefficient, $D_g\delta_g$, has been treated as a fitting parameter in similar way as in [66]. Other parameters have been kept constant during calibration. Their values have been estimated based on literature data.

The relative density evolution obtained in the numerical simulation has been compared with experimental measurements in Fig. 18a and b (please note that the time in these figures is measured from the sintering activation skipping the compaction stage). A reasonably good correspondence between the numerical results and experimental data can be observed. Fig. 18a and b also shows a very good agreement between the viscous and viscoelastic solutions. The coincidence of the viscoelastic solutions obtained for different mass scaling factors confirms the acceptability of mass scaling procedure. Table 5 contains the analysis data showing again the superiority of the viscoelastic model over the standard viscous one.

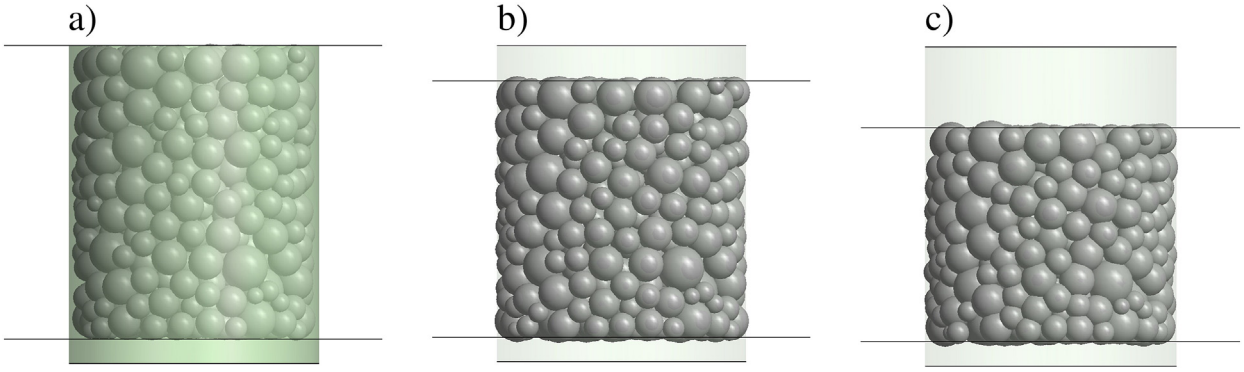

Fig. 17. Numerical simulation of sintering: a) before pressing, b) under pressure, before sintering, c) under pressure, at the end of sintering.

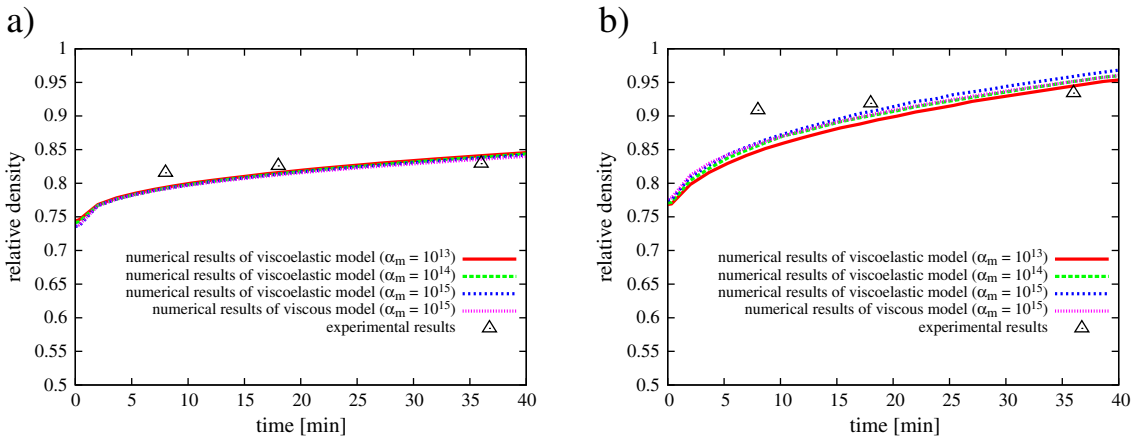

Fig. 18. Evolution of relative density for sintering temperature 1300 °C: pressure 5 MPa, b) pressure 30 MPa.

Table 5
Summary of the analysis data — simulation of sintering of the cylindrical specimen with the mass scaling factor 10^{15}.

Model	Sintering time [s]	Number of time steps	Time step length [s]	CPU [s]	CPU/step [s]
Viscous model	$6 \cdot 10^3$	$1.97 \cdot 10^7$	$3 \cdot 10^{-4}$	$1.24 \cdot 10^4$	$6.3 \cdot 10^{-4}$
Viscoelastic model	$6 \cdot 10^3$	$1.12 \cdot 10^5$	$5.33 \cdot 10^{-2}$	79	$7 \cdot 10^{-4}$

4. Concluding remarks

The new viscoelastic model implemented in the discrete element method has been obtained by adding a spring to the two-particle viscous model of sintering commonly used in the literature. The model reproduces correctly the mechanism of free sintering and sintering under pressure. The results presented in the paper show a big potential of the newly developed viscoelastic model in the simulation of powder sintering processes. While the results obtained using the new model are consistent with the viscous model, the new model offers much better efficiency for the explicit time integration scheme thanks to larger critical time steps. The performance of both models has been compared for similar mass scaling factors. Further extensions of the viscoelastic model are under development.

Acknowledgments

The results presented in this paper have been obtained within the "KomCerMet" project (contract no. POIG.01.03.01-14-013/08-00 with the Polish Ministry of Science and Higher Education) within the framework of the Operational Programme Innovative Economy 2007–2013.

References

[1] M. Abouaf, J.L. Chenot, G. Raisson, P. Bauduin, Finite element simulation of hot isostatic pressing of metal powders, International Journal for Numerical Methods in Engineering 25 (1988) 191–212.
[2] P.C. Angelo, R. Subramanian, Powder Metallurgy: Science Technology and Applications, PHI Learning Pvt, Ltd, 2008.
[3] E. Arzt, The influence of an increasing particle coordination on the densification of spherical powders, Acta Metallurgica 30 (1982) 1883–1890.
[4] M.F. Ashby, A first report on sintering diagrams, Acta Metallurgica 22 (1974) 275–289.
[5] D. Bolster, R.E. Hershberger, R.J. Doneelly, Dynamic similarity, the dimensionless science, Physics Today 9 (2011) 42–47.
[6] P.Z. Cai, D.J. Green, G.L. Messing, Constrained densification of alumina/zirconia hybrid laminates I: experimental observations of processing defects, Journal of the American Ceramic Society 80 (1997) 1929–1939.
[7] P. Ponte Castañeda, The effective mechanical properties of nonlinear isotropic composites, Journal of the Mechanics and Physics of Solids 39 (1991) 45–71.
[8] M. Chmielewski, J. Dutkiewicz, D. Kaliński, L. Litynska-Dobrzynska, K. Pietrzak, A. Strojny-Nedza, Microstructure and properties of hot-pressed molybdenum-alumina composites, Archives of Metallurgy and Materials 57 (2012) 687–693.
[9] M. Chmielewski, D. Kaliński, K. Pietrzak, W. Włosiński, Relationship between mixing conditions and properties of sintered 20AlN/80Cu composite materials, Archives of Metallurgy and Materials 55 (2010) 579–585.
[10] R.L. Coble, Sintering of crystalline solids. I. Intermediate and final state diffusion models, Journal of Applied Physics 32 (1961) 787–792.
[11] A.C.F. Cocks, Inelastic deformation of porous materials, Journal of the Mechanics and Physics of Solids 37 (6) (1989) 693–715.
[12] A.C.F. Cocks, Constitutive modelling of powder compaction and sintering, Progress in Materials Science 46 (2001) 201–229.
[13] J.M. Duva, P.D. Crow, The densification of powders by power-law creep during hot isostatic pressing, Acta Metallurgica et Materialia 40 (1992) 31–35.
[14] H.E. Exner, Principles of single phase sintering, Reviews on Powder Metallurgy and Physical Ceramics 1 (1979) 1–4.
[15] H.E. Exner, E. Arzt, Sintering processes, in: R.W. Cahn, P. Haasen (Eds.), Physical Metallurgy, 30, Elsevier Science, 1996, pp. 2628–2662.
[16] H.E. Exner, T. Kraft, Review on Computer Simulations of Sintering Processes, in: Powder Metallurgy World Congress 1998 (Ed.), 2, EPMA, Shrewsbury, U.K., 1998, pp. 278–283.
[17] J. Frenkel, Viscous flow of crystalline bodies under the action of surface tension, Journal of Physics USSR 9 (1945) 385–391.
[18] S. Gan, J.C. Seferis, R.B. Prime, A viscoelastic description of the glass transition-conversion relationship for reactive polymers, Journal of Thermal Analysis 37 (1991) 463–478.
[19] M. Gasik, B. Zhang, A constitutive model and FE simulation for the sintering process of powder compacts, Computational Materials Science 18 (2000) 93–101.
[20] D. Gendron, PhD thesis Edtude numériqueet expérimentale du frittage a l'echelle du grain, L'Universite Bordeaux I, 2001.
[21] R.M. German, Sintering Theory and Practice, Wiley, New York, 1996.
[22] R.M. German, Computer modeling of sintering processes, Journal of Powder Metallurgy 38 (2002) 48–66.
[23] R.M. German, Critical overview of sintering computer simulations, in: V. Arnhold, C.L. Chu, W.F. Jandeska, H.I. Sanderow (Eds.), Advances in powder metallurgy & particulate materials, Part 9 — ModelingMPIF, Princeton, 2002, pp. 1–15.
[24] T. Hatada, T. Kobori, M. Ishida, N. Niwa, Dynamic analysis of structures with Maxwell model, Earthquake Engineering & Structural Dynamics 29 (2000) 159–176.
[25] B. Henrich, (PhD thesis) (Partikelbasierte Simulationsmethoden in Pulvertechnologie und Nanofluidik), Albert-Ludwigs-Universität Freiburg im Breisgau, 2007.
[26] B. Henrich, A. Wonisch, T. Kraft, M. Moseler, H. Riedel, Simulations of the influence of rearrangement during sintering, Acta Materialia 55 (2007) 753–762.
[27] D.L. Johnson, New method of obtaining volume, grain boundary, and surface diffusion coefficients from sintering data, Journal of Applied Physics 40 (1969) 192–200.
[28] L.C. De Jonghe, M.N. Rahaman, Sintering stress of homogeneous and heterogeneous powder compacts, Acta Metallurgica 36 (1988) 223–229.
[29] D.W. Jung, Study of dynamic explicit analysis in sheet metal forming processes using faster punch velocity and mass scaling scheme, Journal of Materials Engineering and Performance 7 (1998) 479–490.
[30] Y. Hirashima, K. Shinagawa, A constitutive model for sintering of mixed powder compacts, Materials Science Forum 42 (1999) 1041–1046.
[31] R.M. Kadushnikov, V.V. Skorokhod, I.G. Kamenin, V.M. Alievskii, E.Yu. Nurkanov, D.M. Alievskii, Theory and technology of sintering, heat, and chemical heat-treatment processes computer simulation of spherical particle sintering, Powder Metallurgy and Metal Ceramics 40 (3–4) (2001) 154–163.
[32] D. Kaliński, M. Chmielewski, K. Pietrzak, An influence of mechanical mixing and hot-pressing on properties of NiAl/Al2O3 composite, Archives of Metallurgy and Materials 57 (2012) 694–702.

[33] A.V. Khomenko, O.V. Yuschenko, Solid–liquid transition of ultrathin lubricant film, Physical Review E: Statistical, Nonlinear, and Soft Matter Physics 68 (2003) 1–10.
[34] H.G. Kim, O. Gilla, D. Bouvard, A phenomenological constitutive model for sintering of alumina powder, The Journal of the European Ceramic Society 23 (2003) 1675–1685.
[35] W.D. Kingery, M. Berg, Study of the initial stages of sintering of solids by viscous flow, evaporation–condensation and self-diffusion, Journal of Applied Physics 26 (1955) 1205–1212.
[36] D.W. Van Krevelen, Properties of Polymers, Elsevier, 1990.
[37] G.C. Kuczynski, Self diffusion in sintering of metallic particles, Metal Transactions 185 (1949) 169–178.
[38] V. Langlois, X. Jia, Ultrasonic monitoring of the elastic properties of PMMA bead packings and their rearrangement during pressure sintering, Powder Technology 208 (2011) 509–514.
[39] B.A. Latella, T. Liu, High-temperature Young's modulus of alumina during sintering, Journal of the American Ceramic Society 88 (2005) 773–776.
[40] V.A. Levchenko, V.A. Borisenko, Temperature dependence of the elastic modulus of copper and its alloys, Khimicheskoe i Neftyanoe Mashinostroenie 7 (1978) 11–12.
[41] S. Luding, K. Manetsberger, J. Müllers, A discrete model for long time sintering, Journal of Mechanics and Physics of solids 53 (2005) 455–491.
[42] C.L. Martin, L.C.R. Schneider, L. Olmos, D. Bouvard, Discrete element modeling of metallic powder sintering, Scripta Materialia 55 (2006) 425–428.
[43] J.K. McKenzie, R. Shuttleworth, A phenomenological theory of sintering, Proceedings of the Physical Society: B 62 (1949) 833–852.
[44] J.-M. Missiaen, Modelling of sintering: recent developments and perspectives, Revista de Metalurgia Paris 12 (2002) 1009–1019.
[45] E.A. Olevsky, Theory of sintering: from discrete to continuum, Materials Science and Engineering R 23 (1998) 41–100.
[46] L. Olmos, C.L. Martin, D. Bouvard, Sintering of mixtures of powders: experiments and modelling, Powder Technology 190 (2009) 134–140.
[47] C. O'Sullivan, J.D. Bray, Selecting a suitable time step for discrete element simulations that use the central difference time integration scheme, Engineering Computations 21 (2004) 278–303.
[48] E. Oñate, J. Rojek, Combination of discrete element and finite element methods for dynamic analysis of geomechanics problems, Computer Methods in Applied Mechanics and Engineering 193 (2004) 3087–3128.
[49] J. Pan, Modelling sintering at different length scales, International Materials Reviews 2 (17) (2003) 69–85.
[50] F. Parhami, R.M. McMeeking, A network model for initial stage sintering, Mechanics of Materials 27 (1998) 111–124.
[51] A.N.B. Poliakov, P.A. Cundall, Y.Y. Podladchikov, V.A. Lyakhovsky, An explicit inertial method for the simulation of viscoelastic flow: an evaluation of elastic effects on diapiric flow in two- and three-layers models, in: D.B. Stone, S.K. Runcorn (Eds.), Flow and Creep in the Solar System: Observations, Modeling and Theory, Kluwer Academic Publishers, 1993, pp. 175–195.
[52] E. Riande, R. Diaz-Calleja, M.G. Prolongo, R.M. Masegosa, C. Salomon, Polymer Viscoelasticity. Stress and Strain in Practice, Marcel Dekker, Inc., New York, Basel, 2000.
[53] J. Rojek, Modelling and Simulation of Complex Problems of Nonlinear Mechanics Using the Finite and Discrete Element Methods . (in Polish, Habilitation Thesis) Institute of Fundamental Technological Research Polish Academy of Sciences, Warsaw, 2007.
[54] J. Rojek, C. Labra, O. Su, E. Oñate, Comparative study of different discrete element models and evaluation of equivalent micromechanical parameters, International Journal of Solids and Structures 49 (2012) 1497–1517.
[55] J. Rojek, E. Oñate, Multiscale analysis using a coupled discrete/finite element model, Interaction and Multiscale Mechanics 1 (2007) 1–31.
[56] J. Rojek, E. Oñate, F. Zarate, J. Miquel, Modelling of rock, soil and granular materials using spherical elements, In 2nd European Conference on Computational Mechanics ECCM-2001, Cracow, 26–29 June, 2001, 2001.
[57] N.J.A. Sloane, The packing of spheres, Scientific American 250 (1984) 116–125.
[58] P. Sofronis, R.M. McMeeking, Creep of power-law material containing spherical voids, ASME Journal of Applied Mechanics 59 (1992) S88–S95.
[59] J. Sorvari, J. Hämäläinen, Time integration in linear viscoelasticity — a comparative study, Mechanics of Time-dependent Materials 14 (2010) 307–328.
[60] F. Tavarez, M.E. Plesha, Discrete element method for modelling solid and particulate materials, International Journal for Numerical Methods in Engineering 70 (2006) 379–404.
[61] L.M. Taylor, D.S. Preece, Simulation of blasting induced rock motion, Engineering and Computing 9 (2) (1992) 243–252.
[62] C. Thornton, Numerical simulations of deviatoric shear deformation of granular media, 50 (1) (2000) 43–53.
[63] X. Tu, J.E. Andrade, Criteria for static equilibrium in particulate mechanics computations, International Journal for Numerical Methods in Engineering 75 (2008) 1581–1606.
[64] F. Wakai, F. Aldinger, Equilibrium configuration of particles in sintering under constraint, Acta Materialia 51 (2003) 641–652.
[65] W. Weglewski, M. Basista, M. Chmielewski, K. Pietrzak, Modelling of thermally induced damage in the processing of Cr-Al2O3 composites, Composites Part B Engineering 43 (2012) 255–264.
[66] A. Wonisch, T. Kraft, M. Moseler, H. Riedel, Effect of different particle size distributions on solid-state sintering: a microscopic simulation approach, Journal of the American Ceramic Society 92 (2009) 1428–1434.
[67] B. Zhang, M. Gasik, Stress evolution in graded materials during densification by sintering processes, Computational Materials Science 25 (2002) 264–271.